Retinal ganglion cell degeneration is topological but not cell type specific in DBA/2J mice

Tatjana C. Jakobs,[1] Richard T. Libby,[2] Yixin Ben,[1] Simon W.M. John,[2] and Richard H. Masland[1]

[1]Howard Hughes Medical Institute, Harvard Medical School, Boston, MA 02114
[2]Howard Hughes Medical Institute, The Jackson Laboratory, Bar Harbor, ME 04609

Using a variety of double and triple labeling techniques, we have reevaluated the death of retinal neurons in a mouse model of hereditary glaucoma. Cell-specific markers and total neuron counts revealed no cell loss in any retinal neurons other than the ganglion cells. Within the limits of our ability to define cell types, no group of ganglion cells was especially vulnerable or resistant to degeneration. Retrograde labeling and neurofilament staining showed that axonal atrophy, dendritic remodeling, and somal shrinkage (at least of the largest cell types) precedes ganglion cell death in this glaucoma model. Regions of cell death or survival radiated from the optic nerve head in fan-shaped sectors. Collectively, the data suggest axon damage at the optic nerve head as an early lesion, and damage to axon bundles would cause this pattern of degeneration. However, the architecture of the mouse eye seems to preclude a commonly postulated source of mechanical damage within the nerve head.

Introduction

Glaucoma results in a slow, progressive decrease in the population of retinal ganglion cells, the retinal neurons that project to the brain via the optic nerve. It is usually, but not invariably, associated with elevated intraocular pressure. The nature of the mechanistic link between high intraocular pressure and loss of retinal ganglion cells is not firmly established. Although less direct insults have occasionally been suggested, trauma at the optic nerve head, the location where the axons of the ganglion cells join together to leave the globe, has been a leading possibility. Generally speaking, this could occur by compression or by pressure on the axons at their point of exit, but the exact pathophysiological events remain unknown (for reviews see Quigley, 1987, 1999; Libby et al., 2005b; Whitmore et al., 2005).

We reexamined the neural changes that occur during elevated intraocular pressure. We used a mouse model of inherited glaucoma (strain DBA/2J) in which the intraocular pressure is elevated, and the ganglion cells degenerate, with an asynchronous progressive course that in this way resembles the human condition (John et al., 1998; Anderson et al., 2002; Libby et al., 2005a). We had four initial lines of questioning. First, which cell populations are affected? Are only the retinal ganglion cells damaged, or are other retinal neurons damaged as well? Second, are some types of retinal ganglion cells resistant? It is now clear that mouse retinas, like mammalian retinas (generally), contain roughly a dozen distinct physiological types of ganglion cells (Rockhill et al., 2002; Sun et al., 2002a,b; Dacey et al., 2003; Badea and Nathans, 2004; Kong et al., 2005). Previous evidence in humans is commonly interpreted as showing selective loss of large retinal ganglion cells (Quigley et al., 1987, 1988). Is this correct in the mouse model, and, if so, which of the several types of large ganglion cells are affected? Third, is there evidence for interference with axonal transport? This might be expected if the axons were compressed at the nerve head and cytological evidence of blockage is observed in several different species (Quigley and Addicks, 1980). Finally, what can be observed of the sequence of degeneration; i.e., the detailed morphological events that intervene between the normal state and the final degeneration of the ganglion cells?

In various species, all of these questions have been investigated before. Our reasons for restudying them are twofold. First, the mouse model makes it possible to study them in a coordinated way such that the interrelated questions can be studied in parallel in the same retinas from a natural, inherited model of the human disease. Once all of the stages are characterized in mice, mouse genetics will greatly facilitate the characterization of mechanisms affecting each stage. Second, optical imaging and immunocytochemical techniques have evolved during the last few years to a point where neurons of the retina can be visualized with unprecedented precision

Correspondence to Richard H. Masland: masland@helix.mgh.harvard.edu

Abbreviations used in this paper: ChAT, choline acetyltransferase; GABA, γ-aminobutyric acid; GCL, ganglion cell layer; INL, inner nuclear layer; IPL, inner plexiform layer; NOS, nitric oxide synthase; TH, tyrosine hydroxylase.

The Journal of Cell Biology, Vol. 171, No. 2, October 24, 2005 313–325
http://www.jcb.org/cgi/doi/10.1083/jcb.200506099

(MacNeil and Masland, 1998; Gan et al., 2000; Haverkamp and Waessle, 2000; Dacey et al., 2003). We hoped that the improved resolution offered by these advances would provide new clues to the nature of the events that occur during an inherited glaucomatous degeneration.

During the course of the study, we found that degeneration of ganglion cells was not uniformly distributed across the retinal surface. Instead, the retina often presented with radially oriented sectors of degeneration. It is noteworthy that in the human disease, too, the ganglion cell damage is usually not uniformly distributed throughout the whole retina. The leading hypothesis attributes the damaged axon bundles to compression by the rigid collagenous plates of the lamina cribosa. However, the mouse eye appears not to have a lamina cribosa, suggesting a future focus on the trophic role of the glia.

Results

Topography of the degeneration

For every retina, the severity of the glaucomatous damage was assessed by grading the optic nerve on a previously reported three-point scale (mild, moderate, and severe; Anderson et al., 2005; Libby et al., 2005a). Mild-stage nerves can have the minor degree of axon damage that occurs in normal mouse eyes at the studied ages, but they show no evidence of glaucomatous damage and are regarded as unaffected (Anderson et al., 2005; Libby et al., 2005c). By the age of 1 yr, a substantial percentage of DBA/2J mice have developed moderate or severe glaucoma as determined from optic nerve grading. Out of 67 optic nerves that were examined in this study, 19 (28%) showed no indication of glaucomatous damage, 3 (4%) were affected moderately, and 44 (66%) showed signs of severe disease (1 nerve was ungradeable). The progression of the disease in the left and right eyes of any one mouse was not highly correlated. We determined total cell numbers in the ganglion cell layer (GCL) in 29 retinas (4 of which were from 3-mo-old DBA/2J controls) by taking 16× or 25× surveys of the whole-mounted retina and counting the cell nuclei. As expected, the total cell counts corresponded well to the optic nerve grading. In the unaffected retinas, as in the 3-mo-old DBA/2J animals, the total cell density in the central parts of the retina exceeded 9,000 cells/mm^2, which is conforms well with the figure determined previously in normal mice (~8,000 cells/mm^2), tapering off to ~3,000–4,000 cells/mm^2 in the periphery (Jeon et al., 1998). In the most severely affected retinas, we found maximal local cell densities of 6,000 cells/mm^2 (Fig. 1). Interestingly, however, the cell loss was not uniform over the whole area of the retina. In some cases, one or two quadrants were spared from the disease (Fig. 1 B). It was not uncommon, even in retinas with strongly reduced overall ganglion cell counts, to find small sectors of the retina (Fig. 1 C), or at least small islands, that were almost normal. In the most severe cases, the total cell count in the GCL was reduced to a degree such that probably all the remaining cells are amacrine cells (Fig. 1 D). The implications of the spatial anisotropy will be discussed later. To begin, we will describe the neuronal changes that occur during the degeneration.

Starburst amacrine cells are normal in glaucomatous DBA/2J mice

Here, we initially compared vertical sections of a severely affected DBA/2J with a control (C57BL/6J) retina. The reduced

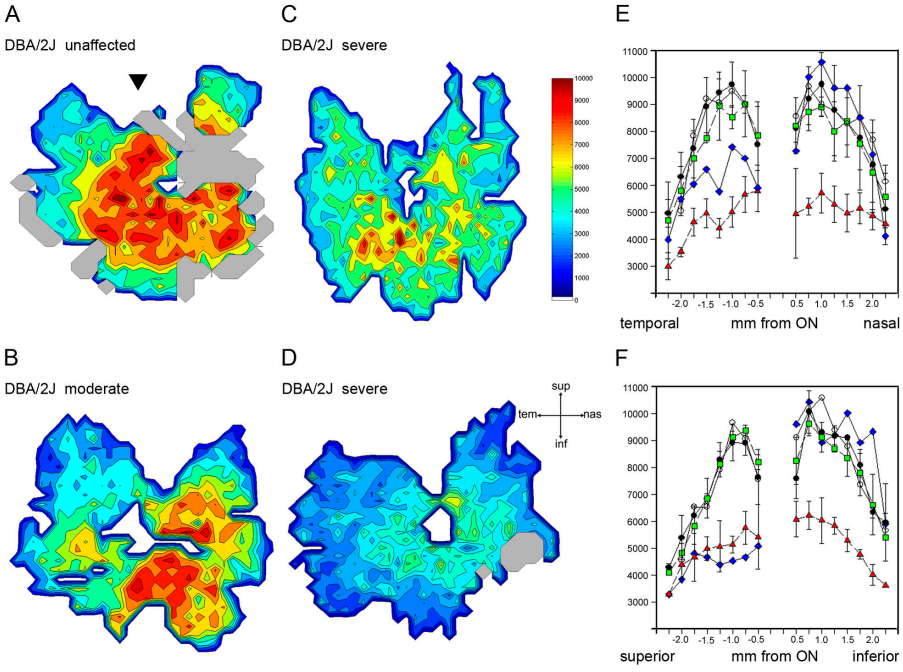

Figure 1. **Neuronal cell counts in the GCL.** (A–D) Total cells in the GCL, excluding endothelial cells and microglia, were counted and graphed as density maps. For easier comparison, all retinas are shown with a temporal to nasal orientation (as if they were all right eyes). The deep cut in the superior pole of the retina (arrowhead) was used for orientation during the preparation. Dark red corresponds to a cell density of 10,000 cells/mm^2, as indicated in the color bar; areas shown in gray could not be counted because of technical reasons. The retina in A (DBA/2J, unaffected optic nerve) shows no sign of degeneration. The retina in B showed moderate glaucoma by optic nerve grading; in this particular case, cell numbers in the nasal half of the retina were severely reduced, whereas the temporal half appears normal. C and D show severe glaucoma by nerve grading. Note that in the retina shown in C, even though the overall cell loss is severe, a region remains with fairly normal cell numbers. (E) Neurons in the GCL were counted along the nasotemporal axis and graphed as cells per millimeter squared. Open circles, C57BL/6J (one retina); black circles, 3-mo-old (predisease) DBA/2J (mean of three retinas ± SEM); green squares, DBA/2J nerve grade unaffected (mean of three retinas); blue diamonds, DBA/2J nerve grade moderate (one retina); red triangles, DBA/2J nerve grade severe (mean of four retinas). (F) GCL neurons along the dorsoventral axis (symbols are the same as in E).

cell density in the GCL was obvious, but otherwise the retinas were indistinguishable (Fig. 2, A and B). In accordance with this, our previous comparison of vertical sections of several severely affected DBA/2J retinas with those of young DBA/2J mice does not support the loss of retinal neurons other than ganglion cells in the majority of eyes (Libby et al., 2005a). These finding argue against heavy loss of neurons other than ganglion cells, but the overall thickness of layers is a coarse method of evaluation. We therefore stained for a variety of amacrine and bipolar cell markers in both whole-mounted retinas and vertical sections, taking the cholinergic starburst type of amacrine cell (Masland et al., 1984) as a well-characterized prototype.

A comparison of cell numbers in the GCL and the number of axons in the optic nerve indicates that >50% of the nuclei in the GCL belong to cells other than ganglion cells; a recent estimate was that the percentage of nonganglion cells was 59 ± 4% of the total (Jeon et al., 1998). We used anti–choline acetyltransferase (ChAT) antibodies to stain the starburst amacrine cells. These cells exist in OFF and ON varieties, with the latter's cell bodies residing in the GCL. Starburst amacrine cells are not the only type of displaced amacrine cell, but they are by far the most numerous and can therefore be used as an index: the loss of these cells proportional to the loss of total cells in the GCL would be indicative of unselective cell loss.

The percentage of all cells in the GCL that were starburst amacrine cells was calculated in 4 central and 4 peripheral fields each from 11 retinas (1 from a C57BL/6J mouse, 2 from 3-mo-old control DBA/2J mice, 3 from unaffected 1-yr-old DBA/2J retinas, and 5 from DBA/2J retinas with severe glaucoma). Starburst cell density and the percentage of cells in the GCL (Fig. 2, E and F) in unaffected retinas corresponded well to the density of these cells in retinas of C57BL/6J mice and in 3-mo-old DBA/2J

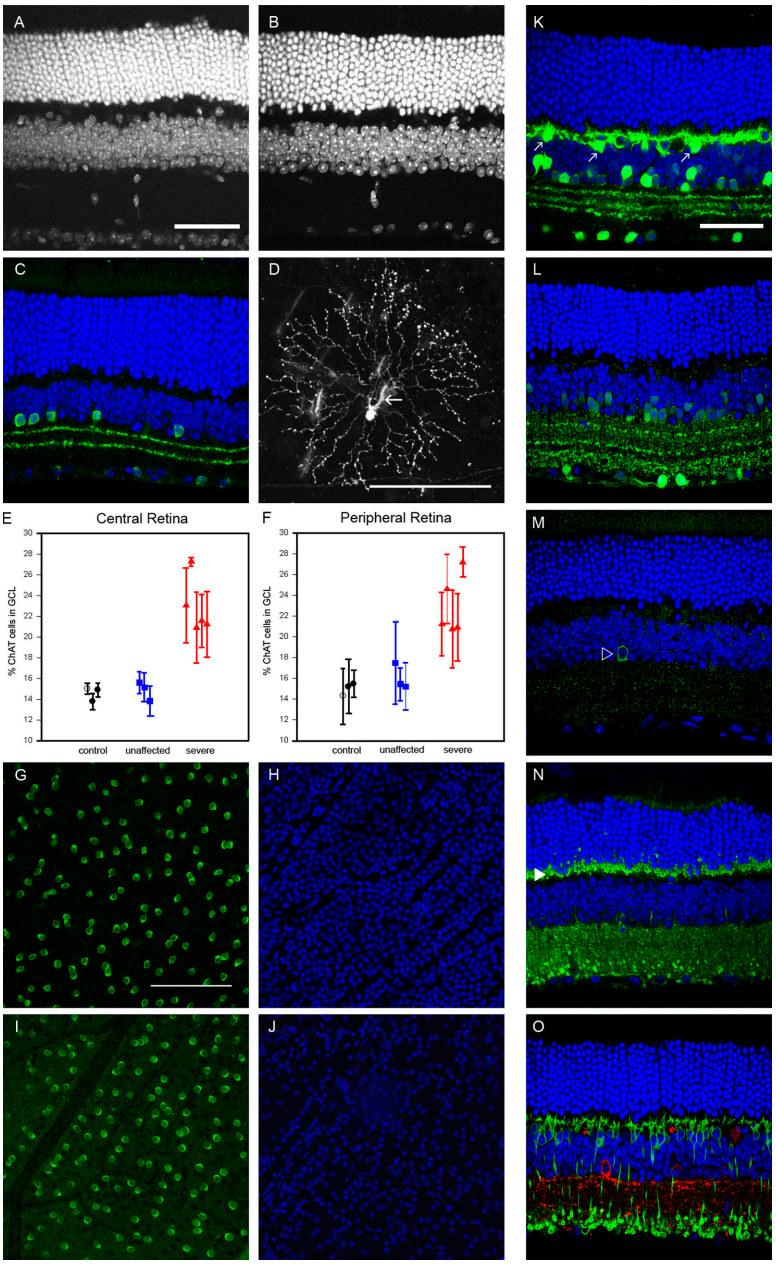

Figure 2. **Amacrine cells in glaucomatous DBA/2J mice.** (A) Single confocal vertical section through the retina of a C57BL/6J mouse, stained with the nuclear dye TOPRO. For the sake of comparison, images in A–C have all been taken in the central part of the retina. (B) Vertical section through a DBA/2J retina (nerve grade severe) under the same conditions. No change in thickness of either the INL or the photoreceptors are observed, but note the sparseness of cell bodies in the GCL in B. (C) Immunostaining for ChAT (green) in a vertical section of a DBA/2J mouse (nerve grade severe) reveals the typical two bands in the IPL and starburst cell bodies in the INL and GCL. (D) Maximum-intensity projection of a stack of 10 confocal sections at 1-μm step size through a starburst amacrine cell labeled biolistically with rhodamine-dextran. The cell shows the characteristic radially symmetric morphology. The arrow indicates a nearby Mueller cell. (E and F) Percentage of ChAT$^+$ amacrine cells of the total cells in the GCL in the central (E) and peripheral (F) retina. Open circles, C57BL/6J; closed circles, 3-mo-old DBA/2J; blue rectangles, DBA/2J nerve grade unaffected; red triangles, DBA/2J nerve grade severe. (G and H) Whole-mounted retina (focus on the GCL) from a 3-mo-old control DBA/2J prediseased animal stained for ChAT (G) and cell nuclei (H). (I and J) Whole-mounted retina from a glaucomatous DBA/2J (nerve grade severe) animal. Though the numbers of ChAT$^+$ starburst amacrine cells in the control and the diseased animals (135 vs. 138 in these two fields) are similar, note the obvious reduction of cells in the GCL in J compared with H. Images in G–J are position matched. (K) Single confocal section of a DBA/2J retina (nerve grade severe) stained for calbindin 28D (green) and cell nuclei (blue). The arrows indicate horizontal cell bodies. Note the sparseness of cell bodies in the GCL in all panels. (L) Staining for GABA (green). (M) Staining for b-NOS (green). The arrowhead indicates a b-NOS$^+$ cell body. (N) Staining for synaptophysin (green). Note the intense synaptic stain in the outer plexiform layer (arrowhead) and throughout the IPL. (O) Staining for PKCα (green) and CD15 (red). The sections in K–O are from the same eye. Bars: (A–C) 50 μm; (D) 50 μm; (G–J) 100 μm; (K–O) 50 μm.

mice (Jeon et al., 1998). In glaucomatous retinas, the percentage of starburst cells was markedly increased, which was indicative of a selective loss of ganglion over amacrine cells. In addition, the diameters of the ChAT-positive cells in the GCLs were measured in the same fields. There were no important differences between affected and unaffected retinas, suggesting that starburst amacrine cells remain morphologically normal. This was further substantiated by the finding that during our labeling of individual ganglion cells with fluorescent dextrans, some starburst cells were occasionally labeled, too. These cells display the characteristic starburst morphology (Fig. 2 D). Finally, vertical sections of a severely affected retina, stained for ChAT, showed the characteristic double band at 40 and 60% of the inner plexiform layer (IPL; Fig. 2 C), which, again, was indistinguishable from unaffected retinas.

Other amacrine cells and rod bipolar cells appear normal in shape and numbers

To test for the possibility of degenerative changes in other retinal neurons, we surveyed a panel of other amacrine cell types for which specific and well-characterized markers are available. This was done in 1-yr-old DBA/2J mice with severe depletion of ganglion cells.

AII amacrine cells are the largest single population of amacrine cells, forming a mandatory interneuron in the pathway from rod photoreceptor to retinal ganglion cells. They constitute a single anatomical and functional type of cell, which plays a pivotal role in vision under dim light conditions (Famiglietti and Kolb, 1975; Strettoi et al., 1992, 1994). In mice, the AII amacrines can be stained with antibodies to the disabled-1 gene product. We calculated the cell density in mid-periphery from whole mounts of two severely glaucomatous eyes to be 2,294 $\pm$ 94 cells/mm^2, which is comparable to the previously published value (Rice and Curran, 2000).

Expression of tyrosine hydroxylase (TH) characterizes a type of widely branching, dopaminergic amacrine cells that stratify in sublaminae 1 and 3 of the IPL and, in addition, send interplexiform branches to the outer plexiform layer (Gustincich et al., 1997). The cells are relatively rare, and their distribution is even over the whole retina. We measured the TH$^+$ cell density in six fields each from a 3-mo-old control animal and a severely affected one. The numbers of TH cells were very similar, with 49.3 $\pm$ 5.5 cells/mm^2 for the control and 48.7 $\pm$ 4.7 cells/mm^2 for the affected retina, respectively. Because these cells are present in low numbers, it was possible to count the total number of TH$^+$ cells in the entire tissue for two retinas. We counted 646 TH cells in a 2-mo-old DBA/2J mouse with a

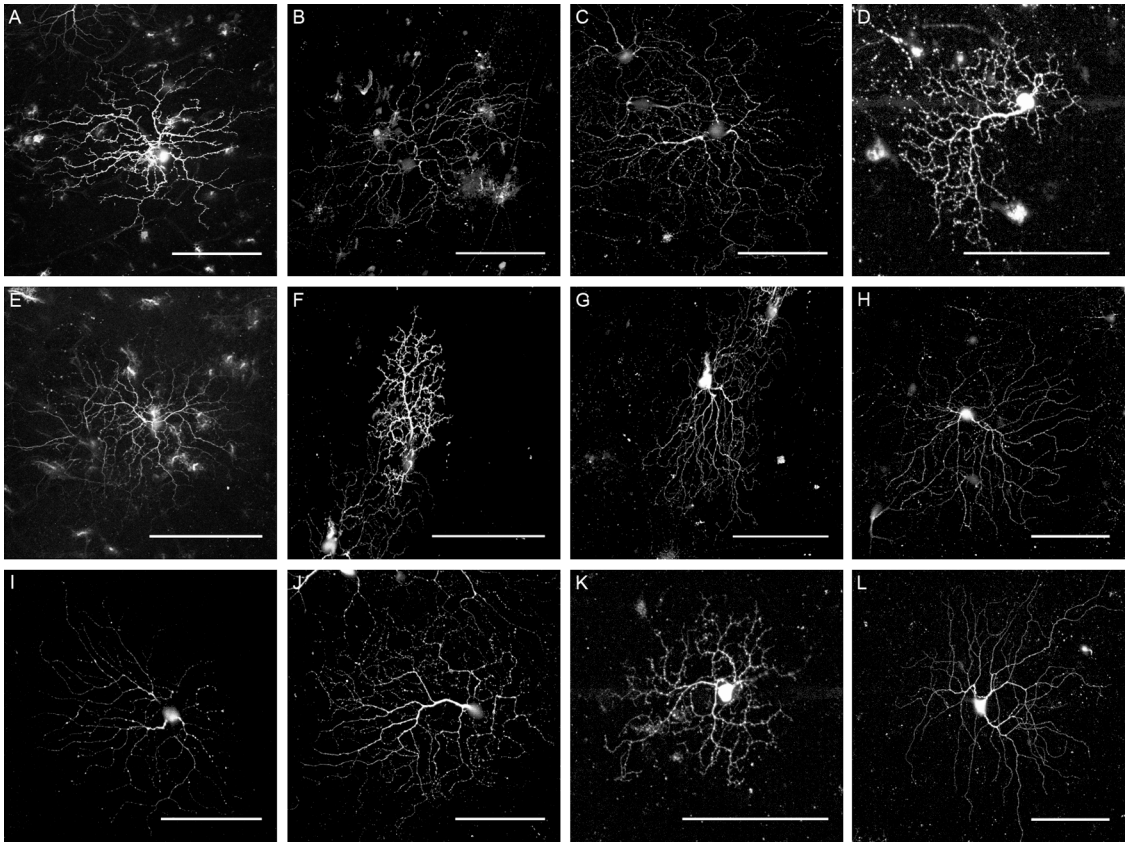

Figure 3. **Gallery of ganglion cell types encountered in glaucomatous DBA/2J.** Individual ganglion cells were labeled either by biolistic delivery of FITC-dextran or by photodynamics. Images represent maximum-intensity projections of 20 confocal sections taken at 1-μm step size. Cells were from moderately or severely affected retinas (based on nerve grade). According to the classification by Sun et al. (2002a), the cells would be classified as follows: (A) type C4; (B) type A2 outer; (C) type C2 inner; (D) type B4; (E) type C5; (F) type B2; (G) type D2 (this cell is bistratified); (H) type A2 inner; (I) type C1; (J) type C2 outer; (K) type C5; and (L) type A1. Bars, 100 μm.

normal nerve and 688 in a retina that was identified as having severe glaucoma by optic nerve grading. The dendrites of the cells, including the extremely fine interplexiform branches, were clearly discernible in the severely affected retina; these cells appear to have suffered no damage of any kind.

These measurements show that there was no quantitative cell loss to the test populations of neurons. In a search for subtle signs of damage, we examined the detailed morphology of several other neuronal populations using antibodies against calbindin D28, b–nitric oxide synthase (NOS), the glycoconjugate epitope CD15, and γ-aminobutyric acid (GABA) as markers. These antibodies label several cell populations of retinal neurons and their processes in the IPL (Versaux-Botteri et al., 1984; Kim et al., 1999; Jakobs et al., 2003). Calbindin D28 is highly expressed in various cell types in the inner nuclear layer (INL) and the GCL and also brightly labels horizontal cells. Calbindin staining of horizontal cells and cells in the INL appeared normal even in severely affected retinas (Fig. 2 K). Immunostaining for the neurotransmitter GABA creates the normal banding pattern in the IPL, in addition to labeling wide-field amacrine cells in both the INL and the GCL (Fig. 2 L). Immunostaining for b-NOS, the synaptic marker synaptophysin, and CD15 on vertical sections revealed no abnormality (Fig. 2, M–O). Finally, the rod bipolar cells, stained with an antibody against PKCα, appeared normal in morphology (Fig. 2 O).

The finding that cell loss is restricted to ganglion cells allows a more accurate estimation of ganglion cell loss. Assuming that amacrine cells in these retinas do not undergo degeneration and that they normally account for 59 ± 4% of the neurons in the GCL (Jeon et al., 1998), the number of actual ganglion cells in the GCL is reduced from the normal value of ~9,000 ganglion cells/mm^2 in the central parts of the retina to <1,000 ganglion cells/mm^2 in the central retina of severely affected retinas.

Types of surviving ganglion cells

There are ≥12 different types of ganglion cells in most mammalian retinas, and each has a distinct function in vision (for review see Masland, 2001). The mouse is no exception to this rule (Sun et al., 2002a; Badea and Nathans, 2004; Kong et al., 2005). We wanted to know if one or a few types of ganglion cells are resistant or particularly vulnerable to degeneration. For this purpose, we closely examined high-resolution serial images of the dendritic and axonal structures from a total of 154 ganglion cells. The cells were visualized either by in vitro photodynamics or by biolistic delivery of fluorescent dextrans, followed by confocal microscopy. Rhodamine-dextran is transported retrogradely from axonal targets into the cell body and can be detected as flu-

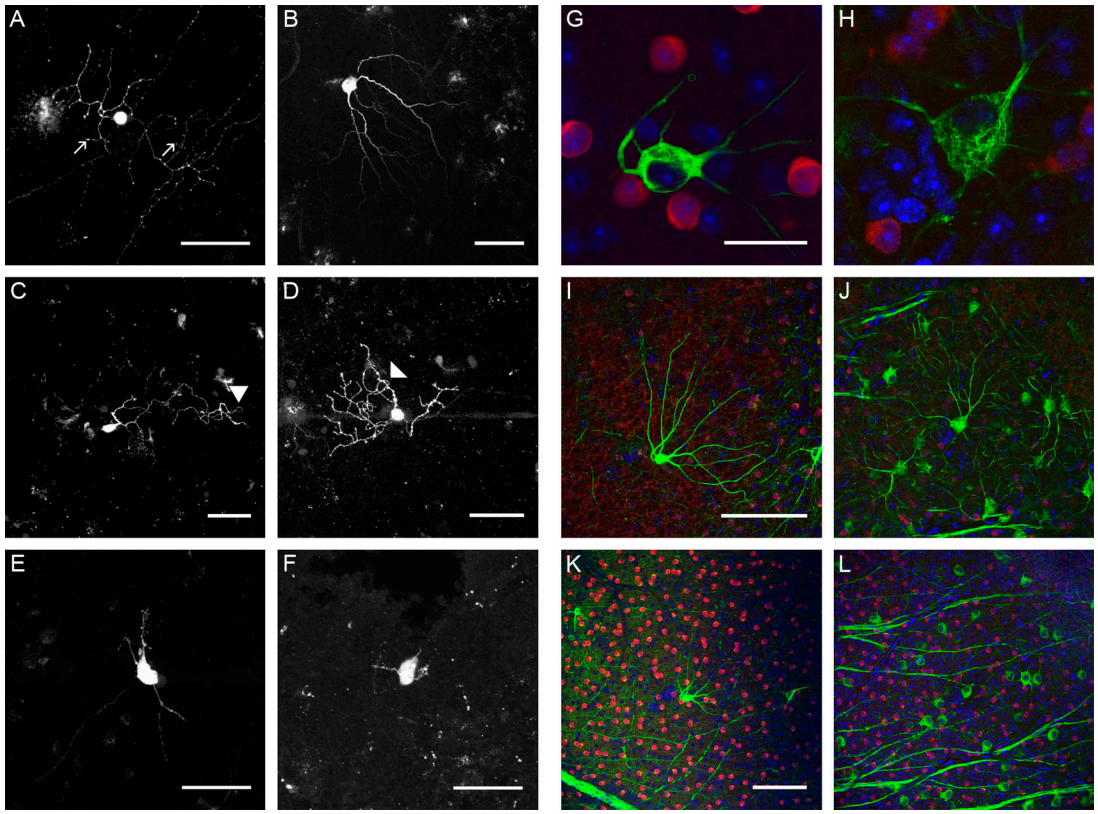

Figure 4. **Affected ganglion cells labeled with the gene gun or SMI32 immunostaining.** (A and B) Affected ganglion cells show a loss of second and higher order dendrites. Only a few and short third order dendrites are visible (arrows). (C and D) These ganglion cells sometimes have long, tortuous dendrites that course in spirals through a considerable portion of the IPL, appearing as loops in the projection image (arrowheads). (E and F) In severely affected ganglion cells, only the cell body and the proximal part of the primary dendrites are visible. (G and H) An affected (G) cell body from a diseased DBA/2J retina (nerve grade severe) at high resolution and a normal SMI32 cell (H) for comparison. SMI32 staining (green), ChAT staining (red), and nuclei staining (blue) are shown. (I and J) The same cells at lower magnification with the dendrites in focus. (K and L) Neighboring cells. Note the loss of SMI32$^+$ cells for the severely affected retina in F. Bars: (A–F) 100 μm; (G and H) 20 μm; (I–L) 100 μm.

orescent granules in the cytosol of the ganglion cells, presumably included in an internal compartment. In addition to indicating axonal transport, this method can be used to image individual cell morphology. Upon photoexcitation, the dye is distributed inside the whole cell, revealing dendrites and axons (Dacey et al., 2003). As this method of "reverse photodynamics" is dependent on intact axons and functioning axonal transport, it can be expected to select for relatively healthy cells. We surveyed all cells labeled in this way ($n = 45$, of which 28 came from affected retinas) to see whether a clear predominance of one or a few cell types could be detected. This would be indicative of the presence of types that are relatively resistant to degeneration. However, in this gallery of ganglion cells we found a wide variety of cell types, just as is observed in the normal mouse.

In addition, we used the gene gun for biolistic delivery of dye-labeled dextrans to the retina. A total of 109 cells were labeled using rhodamine- or FITC-labeled gene gun bullets. Out of these cells, 46 were from moderately to very severely affected retinas and the remainder were from cases in which little or no cell loss was detectable. We saw no evidence for a preponderance of one or a few types in affected retinas, as would have occurred in the case of one or more resistant types. Fig. 3 shows a series of examples of ganglion cells in our sample.

We also looked specifically at two identified types of large retinal ganglion cells. Because of its relative selectivity for α ganglion cells (Drager et al., 1984), SMI32 can also be used to assess preferential vulnerability or resistance of this specific cell type, the largest ganglion cell of all those present in the mouse retina (Peichl et al., 1987; Doi et al., 1995; Sun et al., 2002a; Kong et al., 2005). The total number of brightly labeled $SMI32^+$ cells was counted in 11 retinas from 1-yr-old animals, 6 of which were diagnosed as unaffected by optic nerve grading, and 1 retina from a DBA/2J mouse before the onset of the disease. In the control animal we counted 1,058 SMI32 cells (66.7 cells/mm^2). Similar numbers (68, 59.2, 67.1, 56.1, 44.6, and 52.6 cells/mm^2) were observed in five retinas that were diagnosed as unaffected by optic nerve grading. In the other five retinas, all classified as severe glaucoma by optic nerve grading, the numbers of SMI32 cells were reduced to 26.9, 14, 7, 26.8, 9.1, and 19.7 cells/mm^2, respectively, a reduction to 13.6–40.2% of the number observed in the young control animal.

The photopigment melanopsin characterizes a population of large retinal ganglion cells involved in entraining circadian rhythms (Provencio et al., 1998; Berson et al., 2002; Hattar et al., 2002). An antiserum against melanopsin was used on six retinas in our sample, two of which were diagnosed as severely affected by optic nerve grading, and one 2-mo-old control. The numbers of melanopsin-positive cells (35.5 cells/mm^2 in the control animal) were reduced to 12.5 and 7.1 cells/mm^2 in the severely affected retinas, corresponding to a reduction in melanopsin cells by factors of 4.7 and 2.7, respectively.

The SMI32 and melanopsin cells are among the largest ganglion cells in the mouse retina and, yet, the decrease in their numbers is, if anything, proportionately less than the fall in the total number of ganglion cells, which was >90% in the most severe cases. That they are not differentially lost speaks against a preferential damage to large ganglion cells in this model of glaucoma (indeed, it has been reported that the melanopsin cells are selectively resistant to some causes of degeneration [Robinson and Madison, 2004]).

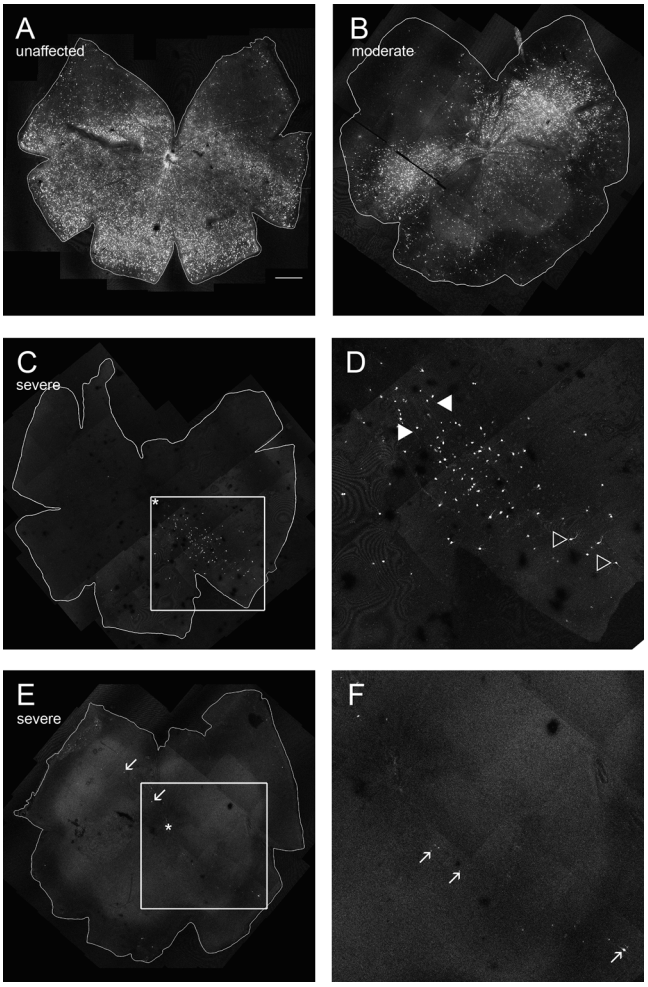

Figure 5. **Low-power views of the whole-mounted retina 1 wk after injection of rhodamine-dextran into the superior colliculus.** The indicated severity refers to optic nerve grade. (A) Typical result in a nondiseased DBA/2J retina. A large, contiguous portion of the surface area is labeled with backfilled cells, which are barely distinguishable at this magnification as individual white dots. Bar, 500 μm. (B) Retina with moderate glaucoma. Two sectors of numerous brightly labeled cells (top right quadrant and bottom left quadrant, top) and less dense smaller sectors (bottom right quadrant) are visible. (C) Retina with severe cell loss. One narrow sector of labeled cells can be clearly seen in the bottom right quadrant. The density of backfilled cells is much lower than in A and B. The optic nerve head is marked by an asterisk. (D) High-resolution view of the boxed area outlined in C. Closed arrowheads point to axons, and open arrowheads indicate two individual backfilled cells whose dendrites are visible even at this magnification. (E) One of the most severely affected retinas in our sample. Hardly any backfilled cells are seen. A tenuous streak of backfilled cells courses from the optic nerve head (asterisk) to the four o'clock position. Another similar streak is visible in the top left quadrant (arrows). (F) High-resolution view of the boxed area outlined in E. The total number of labeled cells in this sector was low (<30), and most cells did not accumulate enough rhodamine-dextran granules to reveal their dendritic morphology. The arrows are the same as in E.

Abnormal ganglion cells

Some of the cells in affected retinas had clearly abnormal morphology (Fig. 4, A–F). Although their numbers varied

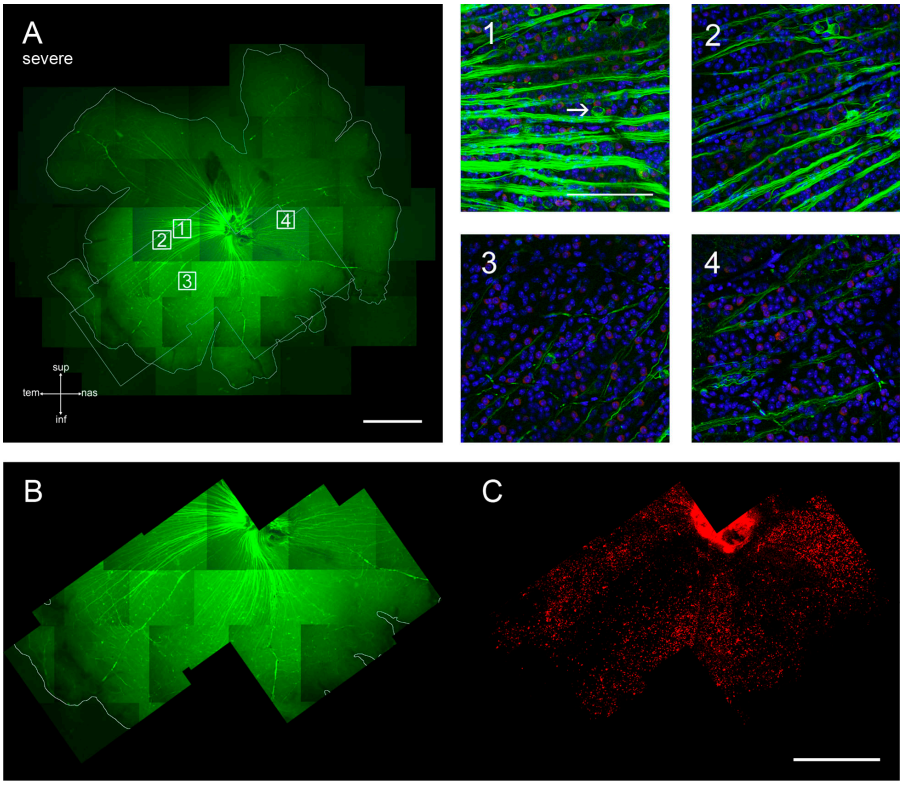

Figure 6. **Sectors of backfilled cells correspond to sectors with relatively many axons.** (A) Low-power view of a retina with moderate glaucoma. The whole mount was stained for the neurofilament marker SMI32, which labels axons and a population of large ganglion cells (green). The outlined squares (fields 1–4) and the outlined irregular box indicate the positions of the higher power insets and of the area in B and C, respectively. The axons and large cell bodies of SMI32$^+$ ganglion cells are shown in green. The arrows in field 1 point to SMI32$^+$ cells. ChAT$^+$ (starburst) amacrine cells are labeled in red, and the cell nuclei are stained with TOPRO (blue). Note the marked difference in the numbers of axons that can be seen traversing the fields. The cell densities in these fields also vary between 7,728 and 7,744 cells/mm^2 in fields 1 and 2 and between 6,352 and 5,936 cells/mm^2 in fields 3 and 4, respectively. Bar, 100 μm. (B) The irregular boxed area from A (stained for SMI32) at higher resolution. (C) The same area as in B, but showing rhodamine-dextran backfill. Individual cell bodies are barely distinguishable as red dots at this magnification. Areas with high numbers of backfilled cells correspond to areas with relatively high numbers of persisting SMI32$^+$ axons. Bar, 500 μm.

from retina to retina, they were a constant feature of all but the most lightly affected tissues. The dendrites of affected cells appeared underbranched. Only primary and secondary dendrites are visible, whereas the higher order branches, usually present on these cells, are lost. Another feature of these cells was the appearance of contorted dendrites that seem to loop and fold back (Fig. 4, C and D, arrowheads), shapes that are never observed in normal ganglion cells. In the most severe cases, only the primary dendrites—sometimes only their proximal segments—were still visible.

As a neurofilament marker, the SMI32 antibody visualizes the cytoskeleton, which appears as a web of filaments around the cell nucleus (Fig. 4 H). In glaucomatous retinas, we observed brightly labeled SMI32 cells whose neurofilaments appear condensed tightly around the nucleus. Dendritic underbranching is especially clear in these cells (Fig. 4, G and I), and sometimes the dendrites do not branch at all.

The cell bodies were shrunken when compared with normal SMI32 cells. We measured the diameters of SMI32 cells in a 3-mo-old retina, three retinas that had escaped the disease, and six severely affected retinas. From each of these 10 retinas, 62 individual cells were measured. The mean diameter of SMI32 cells in the control animal was 20.52 ± 2.6 μm. The diameters in the unaffected DBA/2J retinas were similar to the control: 19.88 ± 1.97, 20.35 ± 2.46, and 20.1 ± 2.84 μm, respectively, which were not significant differences ($P = 0.47$). In five of the glaucomatous retinas, the diameters were significantly smaller (17.07 ± 2.16, 17.1 ± 2.44, 17.09 ± 1.87, 16.27 ± 2.63, and 15.59 ± 2 μm, respectively; $P < 0.001$), corresponding to a shrinkage of between 17 and 25%.

The sixth DBA/2J retina had major ganglion cell loss (nerve grade severe) but had a sector that remained unaffected (see Fig. 10). SMI32 cell diameters were measured for the affected and the normal part of this retina separately. Within the degenerated and normal zones the diameters were 15.8 ± 2.3 and 19.48 ± 2.62 μm, respectively ($P < 0.001$).

Melanopsin-positive ganglion cells were measured in one 3-mo-old control animal and two unaffected and two diseased retinas (34 cells were measured in each case). The cell diameters were as follows: control, 15.58 ± 1.88 μm; unaffected DBA/2J retinas, 15.03 ± 1.87 μm; and severe DBA/2J retinas, 14.8 ± 2.28 μm. This is a small, but statistically significant, degree of shrinkage ($P = 0.0017$).

Axonal abnormalities in ganglion cells

We injected seven 1-yr-old DBA/2J mice, one 2-mo-old DBA/2J mouse, and one C57BL/6J mouse bilaterally into the superior colliculi with rhodamine-dextran and imaged the retinas 1 wk later (Fig. 5). Out of 13 retinas studied, 12 had ganglion cells that contained rhodamine-dextran granules. Four of these retinas were normal. The other nine were moderately to severely affected. As described in the "Types of surviving ganglion cells" section, many of the ganglion cells had normal retrograde transport and normal morphology in the affected retinas. In contrast, those ganglion cells that had abnormal morphology were never seen to contain rhodamine-dextran granules from retrograde transport, indicating that retrograde transport was compromised. Furthermore, the axons of the abnormal ganglion cells appeared shrunken. In normal ganglion cells, the axons are readily visible after retrograde transport of fluorescent tracers or (especially) after staining of neurofilaments with the SMI32

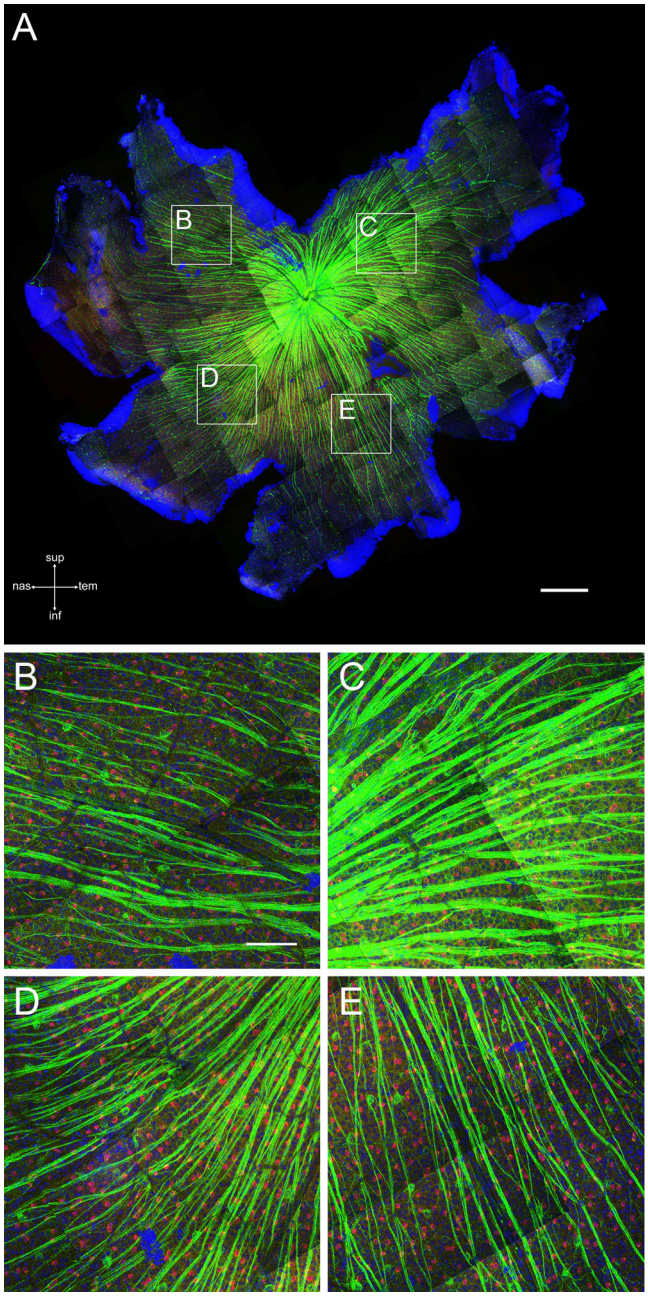

Figure 7. **Whole-mounted unaffected retina.** (A) High-resolution survey of a whole-mounted retina from a DBA/2J retina that had escaped the disease (optic nerve grade unaffected) stained for SMI32 (green) and ChAT (red) and counterstained with TOPRO (blue). Numerous brightly labeled SMI32$^+$ axons are seen all around the optic nerve head and well into the periphery. Bar, 500 μm. (B–E) High-power views of the boxed areas outlined in A. The picture is very similar to that observed in 3-mo-old DBA/2J or in C57BL/6J mice. Bar, 100 μm.

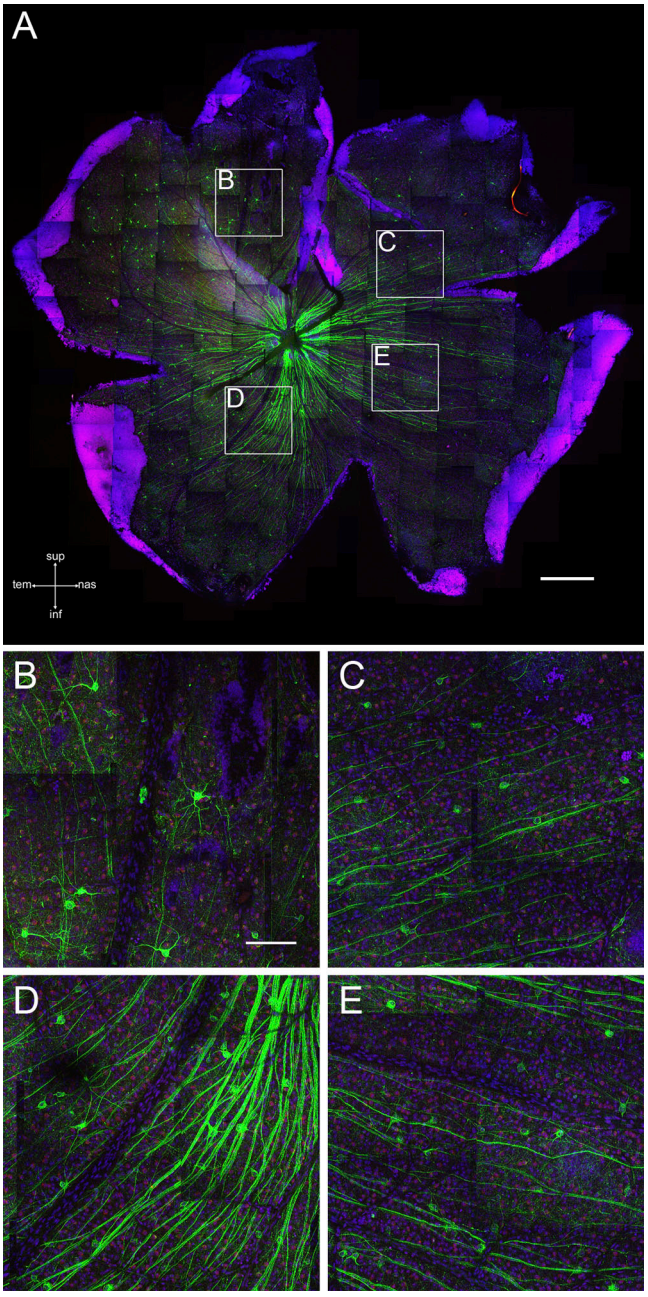

Figure 8. **Whole-mounted glaucomatous retina with persisting sectors of normal appearance.** (A) High-resolution survey of a whole-mounted retina from a moderately affected retina stained for SMI32 (green) and ChAT (red) and counterstained with TOPRO (blue). The axon bundles entering the optic nerve head are markedly reduced and show sectors of relatively high axon densities alternating with sectors with almost no persisting axons. Bar, 500 μm. (B–E) High-power views of the boxed areas outlined in A. Bar, 100 μm.

antibody. In the ganglion cells with remodeled dendrites, the axons were clearly visible only near their exit from the soma; elsewhere, they were so thin as to be virtually invisible.

The sectorial pattern of degeneration

The distribution of the retrogradely labeled cells was unexpected. In normal retinas (C57BL/6J) and in the retina from the young DBA/2J animal, large contiguous parts, usually amounting to ≥50% of the total area, contain labeled cells (the entire retina is not covered because our injections into the superior colliculus do not cover the whole projection field of retinal ganglion cells). In the glaucoma retinas, we found sectors of brightly labeled cells interrupted by sectors that contained no or only very few labeled cells. Fig. 5 shows four examples, with A showing an unaffected retina and B, C, and D showing increasing severity. This result cannot be explained by the injection technique, as the fibers in the

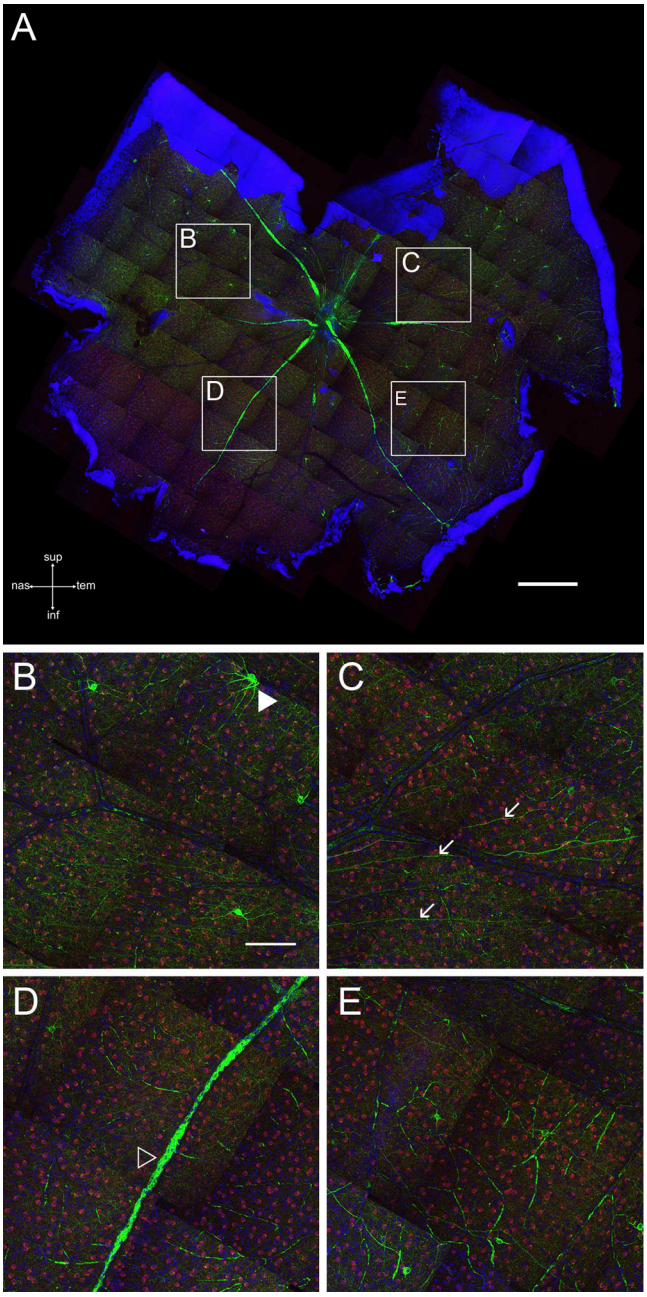

Figure 9. **Whole mount of a severely affected retina with virtually no remaining ganglion cells.** (A) High-resolution survey of a whole-mounted retina from one of the most severely affected eyes in our sample stained for SMI32 (green), ChAT (red), and counterstained with TOPRO (blue). Bar, 500 μm. (B–E) High-power views of the boxed areas outlined in A. Hardly any SMI32$^+$ cells or axons are left. Remaining cells often show long, unbranched dendrites. The open arrowhead in D points to a blood vessel that has been unspecifically labeled by the secondary antibody. The closed arrowhead in B points to an anomalous SMI32$^+$ cell. The arrows in C indicate remaining axons. Note that the ChAT$^+$ cells (red) are unaffected. Bar, 100 μm.

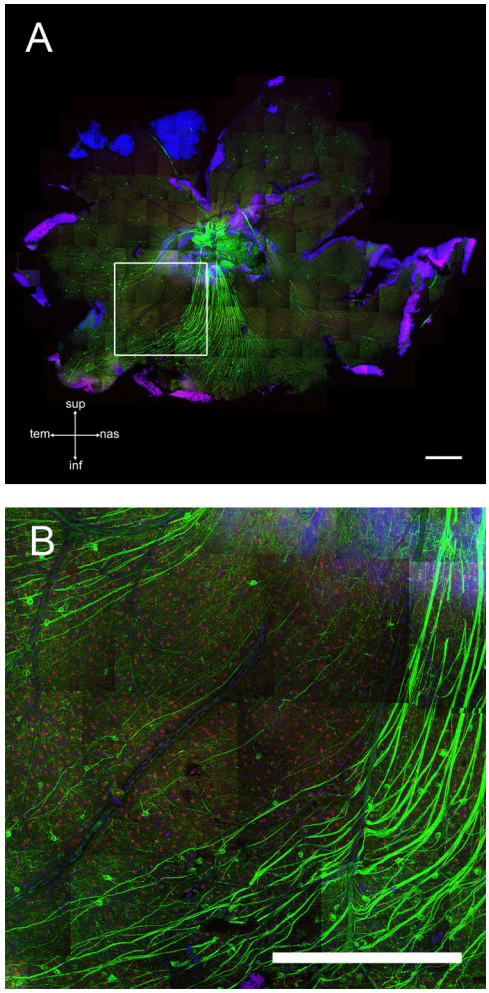

Figure 10. **Sectors of fairly normal ganglion cells can persist even in severe retinas.** (A) Survey of a whole-mounted retina stained with anti-SMI32 (green), Chat (red), and TOPRO (blue). The outlined square indicates the location of the field in B. (B) Higher magnification view. A sharp boundary between an axon- and cell-rich area (bottom) and a depleted area (left) is obvious. The optic nerve grade was severe for this eye. Bars, 500 μm.

superior colliculus are not arranged in this manner, and in normal animals fan-shaped labeling of ganglion cells by retrograde transport is never observed. The areas of backfilled cells correspond to areas where the axon bundles are relatively well preserved, whereas the unlabeled sectors are also denuded of axons (Fig. 6).

This fan-shaped pattern of degeneration was further demonstrated by immunostaining of the whole-mount retinas with an antibody against SMI32. In normal retinas, the SMI32-positive axons completely surround the optic nerve head. In moderately severe disease, the axon bundles are noticeably thinned, and in the most extreme cases, the axons are almost completely lost (see Fig. 7 for a normal, Fig. 8 for an intermediary, and Fig. 9 for an extreme example). SMI32 also reveals that even in otherwise depleted retinas, a sector of almost normal appearance sometimes persists (see Fig. 10 for a striking example).

Discussion

Collectively, these data indicate quite strongly that cell loss and changes in cell morphology are limited to ganglion cells and do not affect other cells in the inner retina, at least at this age in DBA/2J mice. Topographic sectors of retinal ganglion cells degenerate, whereas other regions of retina are spared.

Within those regions, ganglion cells undergo a progression of structural changes that precede frank degeneration. As will be discussed, these patterns contain clues to the mechanism of the degeneration.

Survival of the retinal interneurons

Degeneration of the ganglion cells did not lead to the degeneration of any of the seven populations of amacrine and bipolar cells for which reliable markers are available. From the point of view of synaptic connectivity, this was to be expected. In normal, nonglaucomatous mammals, loss of the ganglion cells causes no degeneration of the afferent neurons, at least within the duration of the usual experiment (Masland et al., 1984; Lin et al., 2004). This is perhaps because the amacrine and bipolar cells under such conditions have lost only a minority of their synaptic targets: most of the synaptic outputs of amacrine and bipolar cells are on other amacrine or bipolar cells, not on ganglion cells. Note the contrast with the situation after photoreceptor degeneration, where the postsynaptic neurons (horizontal and bipolar cells) are almost entirely deprived of synaptic input and major reorganization of their structure occurs (Marc et al., 2003).

The vulnerability of different ganglion cell types

Within the limits of our technique, there was no preference for the degeneration of any one type of retinal ganglion cell. A limitation, of course, is that there are at least a dozen types of retinal ganglion cells in the mouse (Doi et al., 1995; Sun et al., 2002a; Badea and Nathans, 2004; Kong et al., 2005), and the differences between some of them are subtle. This would make it difficult to detect a small numerical difference between the types. That stated, it was clear that a great diversity of types are observed even within severely affected regions, that there was no preponderance of any individual type among the surviving cells, and that there was no bias toward small, medium, or large cells. This was the conclusion when the entire population was surveyed and was supported by further experiments that specifically targeted the α-type cells stained by SMI32 and the unique melanopsin-immunoreactive cells. The SMI32 cells are the largest ganglion cells present in the retina of the mouse, and the melanopsin cells are in the top 25% of soma and dendritic field size. The proportional loss of these cells was not obviously different from the loss of the other types of retinal ganglion cells.

This contrasts with previous evidence that large ganglion cells are selectively vulnerable in human glaucoma (Quigley, 1995, 1999). What is the explanation for this difference? Older studies of human material, which are necessarily much less detailed than those performed here, could have failed to account for the correct populations of neurons in the GCL of the retina, which include many displaced amacrine cells. However, more recent works were certainly aware of this issue, and it would not affect those estimates of ganglion cell size that were based on axon diameter (Quigley et al., 1987, 1988). Another possibility, supported by our results (Fig. 4), is that the apparent loss of large ganglion cells is in fact shrinkage of the cells, so that the average ganglion cell becomes smaller. Such a conclusion was reached (Morgan et al., 2000) from studies in the monkey. None of these studies would explain a report that the magnocellular layers of the lateral geniculate body, which are the target of the largest ganglion cells, suffered a disproportionately greater loss of anterograde axonal transport during experimental glaucoma in a primate model (Dandona et al., 1991). Aside from species differences, the final possibility is that the selective loss of large ganglion cells is in fact a temporal phenomenon in which large ganglion cells are affected first in glaucoma and in small ganglion cells only later. In our study, this is quite possible because we did not intensively investigate early stages of disease, but it would require that the small ganglion cells eventually catch up with the large ones in degenerating.

Retrograde axonal transport

We injected marker compounds into the superior colliculus, and this allowed us to evaluate retrograde transport by the axons of the retinal ganglion cells. Additionally, the soma and dendritic structure of the cell could be visualized and compared with cells visualized by other means such as immunocytochemistry or particle-mediated cell filling. We sought evidence comparing the time course of the degeneration with the presence or absence of axonal transport. Because this was a correlative study, the results do not demonstrate causation, but there were interesting new findings.

One the one hand, retrograde transport is not generically impaired, as many ganglion cells could be successfully filled with marker compounds by retrograde transport from the superior colliculus. In incompletely affected retinas (those with many surviving ganglion cells), these surely included neurons destined eventually to degenerate. Thus, there was no evidence for a long period during which retrograde transport is compromised but the soma and dendrites survive.

On the other hand, we did observe partially degenerated cells, most clearly in SMI32 staining. They had truncated and misdirected dendrites, shrunken somata, abnormal accumulation of neurofilaments, and exceptionally thin axons. These cells were never observed to be filled by retrograde transport. Thus, the failure of axonal transport and a generalized neuronopathy occur at more or less the same time in these mice. The partially degenerated (perhaps remodeled is a better term) state of these ganglion cells is of some interest. It appears to reflect a stable state in which the cells have simplified their dendritic arbors but have not yet embarked on apoptosis. There is little cytological evidence of immanent cell death: for example, the dendrites appear smooth, in contrast to their jagged or beaded appearance in severely damaged neurons. This suggests that the cells have suffered an insult but retain their fundamental homeostatic mechanisms (Whitmore et al., 2005). Aside from its cell biological interest, such a state might provide an opportunity for therapeutic rescue in the human disease.

Sectors of ganglion cell degeneration

From our results and many others it seems likely that the fundamental insult after high intraocular pressure happens at the optic nerve head. If elevated intraocular pressure were itself damaging, other retinal neurons (amacrine and/or bipolar cells) as well as ganglion cells may be damaged. Arguing against a direct dam-

aging effect of pressure, this was not the case for the several populations of amacrine and bipolar cells that we can stain. Furthermore, because the intraocular pressure is distributed more or less evenly throughout the globe, ganglion cells should be damaged throughout the retina, which was not the case. All of these results are consistent with the lesion being initiated at or near the point where the axons leave the eye.

A striking finding was that radiating, fan-shaped sectors of ganglion cells degenerated. The sectors had their narrowest point near the optic nerve head and widened peripherally. Within the degenerated zone, there was no readily apparent central to peripheral gradient; in other words, ganglion cell degeneration was more or less equally severe at all eccentricities within the zone. This geometry is hard to attribute to a pathology other than a focal insult to groups of neighboring axons within the optic nerve head, which must create a widening zone of axons as they radiate away from the optic nerve head.

What might that insult be? In the human disease, as in the mouse, the loss of ganglion cells is restricted to coherent zones; it is far from a random dropping out of individual ganglion cells (in humans, the axons curve as they radiate away from the nerve head; this is what creates the arcuate scotoma of glaucoma). In the human disease, the degeneration is often attributed to pressure of the rigid collagenous matrix of the lamina cribrosa against the optic nerve axons. As bundles of axons pass through openings in the lamina cribrosa, they are thought to be mechanically constricted in bundles that are defined by the distinct apertures through which they pass between the laminar plates.

Optic nerve excavation, a hallmark of human glaucoma, is observed in the DBA/2J mice (Anderson et al., 2005; Libby et al., 2005a). By analogy with thinking about the human disease, we first hypothesized that bundles of axons are collectively damaged during their passage through apertures in the lamina cribrosa. It is not hard to imagine bundles of axons being strangled where they pass together through a pathologically narrowed opening. However, it appears that the connective tissue meshwork present in primates does not exist in the mouse (May and Lutjen-Drecoll, 2002; unpublished data). This seems to exclude a purely mechanical event involving the connective tissue plates of the lamina cribrosa as the basis of damage to axon bundles in the mouse.

The optic nerve of the mouse is nonetheless fasciculated with, instead of rigid connective tissue, a sheath of glial cells delineating each bundle of axons (Morcos and Chan-Ling, 2000). It is possible that these bundles are the physical substratum of the islands of sparing or damage observed during glaucomatous damage (the elementary unit that is either damaged or spared). Conceivably, something in the behavior of the ensheathing glial cells triggers damage during elevated intraocular pressure (Neufeld, 1999; Morgan, 2000; Neufeld and Liu, 2003). Alternatively, the glia could actually have a positive function for the axon bundles they surround, protecting specific bundles of ensheathed axons from damage caused by another cause. Our results thus suggest an increased focus on the cell biological interactions between optic axons and their surrounding astrocytes, such as local trophic events.

Materials and methods

Preparation of the retinas and optic nerves

All animal procedures were approved by our Institutional Animal Care and Use Committees. 1-yr-old DBA/2J mice were used for most experiments. For strain-matched controls, we used 2-mo-old DBA/2J mice (an age before the onset of the disease). C57BL/6J mice aged 2 mo and 1 yr were used as additional controls. The mice were bred and aged at the Jackson Laboratory with diet and housing conditions as previously described (John et al., 1998). The light-adapted mice were anesthetized with isoflurane and killed by an i.p. injection of 100 mg/kg ketamine and 20 mg/kg xylazine in accordance with the Subcommittee on Research Animal Care of the Massachusetts General Hospital guidelines. Before removal of the eye, the superior pole was marked with a low-temperature electrical cautery (Aaron Medical Industries). The eyeball was exposed, and the optic nerve was cut intraorbitally with sharp scissors. The eyes were removed and hemisected along the ora serrata. The upper pole was marked with a long incision. The retinas were separated from the pigment epithelium and mounted ganglion cell side up on Isopore 3-μm (Millipore) filters using smaller cuts in the periphery to flatten the retina. All of these manipulations were done in oxygenated mammalian Ringer's solution. In parallel, the animal's brain was exposed, and a scalpel blade was used to cut away the brain parallel to the skull base, leaving the optic chiasm and 1–2 mm of overlying tissue in place. The head was immersed in fixative (0.8% formaldehyde and 1.22% glutaraldehyde) for 24 h and washed in 0.1 M phosphate buffer and stored in cold phosphate buffer for later analysis of the optic nerves.

Ganglion cell labeling

Biolistic transfer of dye-coupled dextran or in vitro photodynamics (Dacey et al., 2003) or a combination of both was used to label ganglion cells. For biolistic labeling, the retinas were prepared as described in the previous section, and two or three rounds of tungsten bullets coated with rhodamine- or FITC-labeled dextran (MW 3000; Invitrogen) were fired using a gene gun system (Helios; Bio-Rad Laboratories) at 120 psi. This device was originally developed to introduce DNA or RNA into living tissue, but it can also be used for delivery of other molecules (Gan et al., 2000). We used fixable dextrans because these molecules stay confined in the cell, and the labeling survives mild treatment with detergents. The dye incorporation by this method is nonselective. In addition to ganglion cells, other components of the GCL, including the displaced amacrine cells and Mueller cell feet, are labeled. In our sample, we identify a cell as a ganglion cell only when at least the initial segment of the axon could clearly be identified. Rhodamine- or FITC-labeled dextran was coated onto 1.1-μm tungsten bullets as follows: (a) the dextran was dissolved in water at 0.2 μg/μl and mixed with 40–50 mg of tungsten bullets; (b) the mixture was spread on a microscope slide, dried, and resuspended in absolute ethanol; (c) the bullets were sonicated for 5 min and passed through 20- and 5-μm pore filters; and (d) polyvinylpyrolidone was added to a final concentration of 0.005 mg/ml. This was used to coat Tefzel tubing for gene gunning in accordance with the manufacturer's instructions.

For in vitro photodynamics, the mice received bilateral injections into the superior colliculi. The animals were anesthetized, and small craniotomies were performed over the superior colliculi. 0.5–1 μl of rhodamine-labeled dextran was injected using a glass capillary mounted on a micromanipulator equipped with a micropipette holder and connected to a Picospritzer II (General Valve Corporation). The craniotomies were filled with Gelfoam (Upjohn), and the skin was closed with surgical clips. 5–6 d later, the animals were killed. The retinas were prepared as described in the previous section and exposed to illumination at 620 nm under optical control. When the dendritic morphology of the cell was clearly visible, the retinas were either fixed or exposed to an additional labeling, this time using the gene gun and FITC-labeled dextran.

Directly after gene gunning or reverse photodynamics, the retinas were fixed in 4% PFA/0.1 M phosphate buffer for 30 min and washed in three changes of phosphate buffer. Individual ganglion cells were imaged on a confocal microscope (Radiance; Bio-Rad Laboratories) using an objective (25×/0.8 Plan-Apochromat; Carl Zeiss MicroImaging, Inc.) and appropriate zoom settings. A z-series was taken through each cell at 1-μm steps from the border of the INL to the GCL. Survey pictures of the whole mount were taken at 10× (10×/0.3 Plan-Neofluar; Carl Zeiss MicroImaging, Inc.). The retinas were counterstained with DAPI, and survey pictures were taken on an Axioscope (Carl Zeiss MicroImaging, Inc.) using an objective (16×/0.5 Plan-Neofluar; Carl Zeiss MicroImaging, Inc.). Covering the whole retina in this way required ~80 individual images of 1,315 × 1,033 pixels, corresponding to a final magnification of 55.89.

Imaging individual ganglion cells

A through-focus series (z-step size, 1 μm) of images of each labeled cell was taken with a confocal microscope equipped with a krypton-argon laser using the 25×/0.8 objective. Each image in the stack was saved as a bitmap. The sections spanning the dendritic arbor (usually 10–15 sections, depending on the stratification of the cell) were exported into Matlab 6.5 (The Mathworks) and a maximum intensity projection of the image stack was created. The resulting single image was thresholded at a pixel intensity of 40. In some cases, image intensity and contrast were adjusted in Photoshop 7 (Adobe Systems, Inc.). No other image processing was done.

Immunohistochemistry

Antibodies against ChAT, TH, and PKCα were obtained from Chemicon. The mouse anti-SMI32 mAb was purchased from Sternberger Monoclonals. The rabbit polyclonal antiserum to melanopsin was a gift from K.-W. Yau (Johns Hopkins School of Medicine, Baltimore, MD; Hattar et al., 2002). Because the retinas had to be studied first in the living state and then after fixation, the mice could not be perfused before the experiments. We therefore occasionally observed unspecific labeling of blood vessels with the secondary antibody used to detect the anti-SMI32 mAb. This labeling could clearly be distinguished from components of the neural retina and did not interfere with imaging.

The whole mounts were incubated with the primary antibodies for 7 d at 4°C, washed, and incubated for 2 d with FITC- or rhodamine-labeled secondary antibodies (all from Jackson ImmunoResearch Laboratories) and counterstained with TOPRO-3 iodide (Invitrogen). They were then mounted with Vectashield (Vector Laboratories) and evaluated on a confocal microscope. A 25×/0.8 objective was used for taking surveys of the whole-mounted retina. These were montaged from ~180 single pictures of 512 × 512 pixels, corresponding to a final magnification of 37×. Many of the illustrations show such montages, readily identifiable by the slightly different exposures in each of the individual micrographs. Although more tedious than taking only a few, very low power survey pictures, the high resolution of the montage allowed recovery of detailed cellular information at later times.

Water immersion lenses (C-Neofluar 40×/1.2 and C-Neofluar 63×/1.4; Carl Zeiss MicroImaging, Inc.) were used for high resolution imaging of single cells. The emission filters were 522DF35 for FITC, 680DF32 for TOPRO-3, and 605DF32 for rhodamine. Alignment for all channels was confirmed by imaging 4- and 0.5-μm fluorobeads (TetraSpeck; Invitrogen) at settings identical to those used for imaging.

Amacrine and bipolar cells were evaluated in vertical sections in addition to whole mounts. For this, retinas were fixed and embedded in 4% agarose, and 30–50-μm sections were cut on a vibratome. The sections were incubated with appropriate amounts of primary antibody overnight at RT and with the secondary antibodies for several hours. After counterstaining with TOPRO-3, the sections were mounted and evaluated under the confocal microscope essentially as described above.

Cell counting and measurement

All cell counting and measurement was performed by an investigator ignorant of the results of optic nerve scoring (see below) and vice versa. Full resolution pictures of the whole-mount retina were assembled from individual pictures in Photoshop 7. No image processing was performed on the individual images. These montages were used for archiving the results, counting cells, and generating lower resolution figures. The complete resolution montage was covered with a counting grid of 22 × 22 squares of 20,164 pixels^2 corresponding to 18.225 × 10^{-3} mm^2 on the original micrograph. The numbers of SMI32-, melanopsin-, or ChAT-positive cells and the TOPRO-3–stained total cell nuclei were counted per grid square. Cell nuclei on the edge of the square were included if the nucleolus was visible. Endothelial cell nuclei were easily recognizable by their elongated shape and were not counted. The raw counts were converted into cells/millimeter^2 and rendered as a two-dimensional density map by a routine written in Matlab 6.5.

The DAPI-stained whole mounts were assembled in the same fashion. Cell bodies in the GCL were counted using a grid at a finer resolution (36 × 36 squares of 20,164 pixels^2, corresponding to 7.744 × 10^{-3} mm^2) and processed as in the previous paragraph. Mean diameters of immunostained cells were determined from the assembled whole mounts or from vertical sections. The widest diameter was measured on digital micrographs using SigmaScan (Jandel Scientific). The measurements were tested for differences by analysis of variance, using the appropriate Matlab routines.

For quantification of cell populations, most of our studies used direct counting of the stained cell populations of retinal surface. In addition, an independent estimate of the overall severity of ganglion cell degeneration could be obtained by optic nerve staining. This method does not convey topographic differences in ganglion cell degeneration, but the values provide a link to previous work and a simple summary of the degeneration's overall severity. In brief, optic nerves were fixed overnight in situ, dissected free, embedded in plastic, and sectioned. Sick and dying axons were differentiated from healthy axons using staining with paraphenylenediamine, which accumulates in sick and dying axons (Anderson et al., 2005; Libby et al., 2005c). These sections were graded by two and sometimes three independent, blinded observers, using an explicit grading scale to determine the level of glaucomatous damage for each eye (Libby et al., 2005a). It divided the continuum of glaucomatous damage into three components: mild, moderate, and severe. Mild nerves were judged to have no glaucomatous axonal damage and are classified as unaffected. Moderate nerves were judged to have between 5 and 50% of the axons damaged or lost. Severe nerves were judged to have >50% axonal damage and/or loss.

We wish to thank Richard Smith and Larry Wilson for excellent assistance.

S.W.M. John and R.H. Masland are investigators of the Howard Hughes Medical Institute. R.H. Masland is a Senior Investigator of Research to Prevent Blindness.

Submitted: 16 June 2005
Accepted: 6 September 2005

References

Anderson, M.G., R.S. Smith, N.L. Hawes, A. Zabaleta, B. Chang, J.L. Wiggs, and S.W.M. John. 2002. Mutations in genes encoding melanosomal proteins cause pigmentary glaucoma in DBA/2J mice. *Nat. Genet.* 30:81–85.

Anderson, M.G., R.T. Libby, D.B. Gould, R.S. Smith, and S.W. John. 2005. High-dose radiation with bone marrow transfer prevents neurodegeneration in an inherited glaucoma. *Proc. Natl. Acad. Sci. USA.* 102:4566–4571.

Badea, T.C., and J. Nathans. 2004. Quantitative analysis of neuronal morphologies in the mouse retina visualized by using a genetically directed reporter. *J. Comp. Neurol.* 480:331–351.

Berson, D.M., F.A. Dunn, and M. Takao. 2002. Phototransduction by retinal ganglion cells that set the circadian clock. *Science.* 295:1070–1073.

Dacey, D.M., B.B. Peterson, F.R. Robinson, and P.D. Gamlin. 2003. Fireworks in the primate retina: in vitro photodynamics reveals diverse LGN-projecting ganglion cell types. *Neuron.* 37:15–27.

Dandona, I., A. Hendrickson, and H.A. Quigley. 1991. Selective effects of experimental glaucoma on axonal transport by retinal ganglion cells to the dorsal lateral geniculate nucleus. *Invest. Ophthalmol. Vis. Sci.* 32:1593–1599.

Doi, M., Y. Uji, and H. Yamamura. 1995. Morphological classification of retinal ganglion cells in mice. *J. Comp. Neurol.* 356:368–386.

Drager, U.C., D.L. Edwards, and C.J. Barnstable. 1984. Antibodies against filamentous components in discrete cell types of the mouse retina. *J. Neurosci.* 4:2025–2042.

Famiglietti, E.V.J., and H. Kolb. 1975. A bistratified amacrine cell and synaptic circuitry in the inner plexiform layer of the retina. *Brain Res.* 84:293–300.

Gan, W.-B., J. Grutzendler, W. Wong, R. Wong, and J. Lichtman. 2000. Multicolor "DiOlistic" labeling of the nervous system using lipophilic dye combinations. *Neuron.* 27:219–225.

Gustincich, S., A. Feigenspan, D.K. Wu, L.J. Koopman, and E. Raviola. 1997. Control of dopamine release in the retina: a transgenic approach to neural networks. *Neuron.* 18:723–736.

Hattar, S., H.-W. Liao, M. Takao, D.M. Berson, and K.-W. Yau. 2002. Melanopsin-containing retinal ganglion cells: architecture, projections, and intrinsic photosensitivity. *Science.* 295:1065–1070.

Haverkamp, S., and H. Waessle. 2000. Immunocytochemical analysis of the mouse retina. *J. Comp. Neurol.* 424:1–23.

Jakobs, T.C., Y. Ben, and R.H. Masland. 2003. CD15 immunoreactive amacrine cells in the mouse retina. *J. Comp. Neurol.* 465:361–371.

Jeon, C.-J., E. Strettoi, and R.H. Masland. 1998. The major cell populations of the mouse retina. *J. Neurosci.* 18:8936–8946.

John, S.W., R.S. Smith, O.V. Savinova, N.L. Hawes, B. Chang, D. Turnbull, M. Davisson, T.H. Roderick, and J.R. Heckenlively. 1998. Essential iris atrophy, pigment dispersion, and glaucoma in DBA/2J mice. *Invest. Ophthalmol. Vis. Sci.* 39:951–962.

Kim, I.B., E.J. Lee, K.Y. Kim, W.K. Ju, S.J. Oh, C.K. Joo, and M.H. Chun. 1999. Immunocytochemical localization of nitric oxide synthase in the mammalian retina. *Neurosci. Lett.* 267:193–196.

Kong, J.H., D.R. Fish, R. Rockhill, and R.H. Masland. 2005. Diversity of gan-

glion cells in the mouse retina: unsupervised morphological classification and its limits. *J. Comp. Neurol.* 489:293–310.

Libby, R.T., M.G. Anderson, I.-H. Pang, Z. Robinson, O.V. Savinova, I.M. Cosma, A. Snow, L.A. Wilson, R.S. Smith, A.F. Clark, and S.W.M. John. 2005a. Inherited glaucoma in DBA/2J mice: pertinent disease features for studying neurodegeneration. *Vis. Neurosci.* In press.

Libby, R.T., D.B. Gould, M.G. Anderson, and S.W. John. 2005b. Complex genetics of glaucoma susceptibility. *Annu. Rev. Genomics Hum. Genet.* 6:15–44.

Libby, R.T., Y. Li, O.V. Savinova, J. Barter, R.S. Smith, R.W. Nickells, and S.W.M. John. 2005c. Susceptibility to neurodegeneration in a glaucoma is modified by bax gene dosage. *PLoS Genet.* 1:e4.

Lin, B., S.W. Wang, and R.H. Masland. 2004. Retinal ganglion cell type, size, and spacing can be specified independent of homotypic dendritic contacts. *Neuron.* 43:475–485.

MacNeil, M.A., and R.H. Masland. 1998. Extreme diversity among amacrine cells: implications for function. *Neuron.* 20:971–982.

Marc, R.E., B.W. Jones, C.B. Watt, and E. Strettoi. 2003. Neural remodeling in retinal degeneration. *Prog. Retin. Eye Res.* 22:607–655.

Masland, R.H. 2001. The fundamental plan of the retina. *Nat. Neurosci.* 4:877–886.

Masland, R.H., J.W. Mils, and S.A. Hayden. 1984. Acetylcholine-synthetizing amacrine cells: identification and selective staining by using autoradiography and fluorescent markers. *Proc. R. Soc. Lond. B. Biol. Sci.* 223:79–100.

May, C.A., and E. Lutjen-Drecoll. 2002. Morphology of the murine optic nerve. *Invest. Ophthalmol. Vis. Sci.* 43:2206–2212.

Morcos, Y., and T. Chan-Ling. 2000. Concentration of astrocytic filaments at the retinal optic nerve junction is coincident with the absence of intra-retinal myelination: comparative and developmental evidence. *J. Neurocytol.* 29:665–678.

Morgan, J.E. 2000. Optic nerve head structure in glaucoma: astrocytes as mediators of axonal damage. *Eye.* 14:437–444.

Morgan, J.E., H. Uchida, and J. Caprioli. 2000. Retinal ganglion cell death in experimental glaucoma. *Br. J. Ophthalmol.* 84:303–310.

Neufeld, A.H. 1999. Nitric oxide: a potential mediator of retinal ganglion cell damage in glaucoma. *Surv. Ophthalmol.* 43:S129–S135.

Neufeld, A.H., and B. Liu. 2003. Glaucomatous optic neuropathy: when glia misbehave. *Neuroscientist.* 9:485–495.

Peichl, L., H. Ott, and B.B. Boycott. 1987. Alpha ganglion cells in mammalian retinae. *Proc. R. Soc. Lond. B. Biol. Sci.* 231:169–197.

Provencio, I., G. Jiang, W.J. De Grip, W. Paer Hayes, and M.D. Rollag. 1998. Melanopsin: an opsin in melanophores, brain, and eye. *Proc. Natl. Acad. Sci. USA.* 95:340–345.

Quigley, H.A. 1987. Reappraisal of the mechanisms of glaucomatous optic nerve damage. *Eye.* 1:318–322.

Quigley, H.A. 1995. Ganglion cell death in glaucoma: pathology recapitulates ontogeny. *Aust. N. Z. J. Ophthalmol.* 23:85–91.

Quigley, H.A. 1999. Neuronal death in glaucoma. *Prog. Retin. Eye Res.* 18:39–57.

Quigley, H.A., and E.M. Addicks. 1980. Chronic experimental glaucoma in primates. II. Effects of extended intraocular pressure on optic nerve head and axonal transport. *Invest. Ophthalmol. Vis. Sci.* 19:137–152.

Quigley, H.A., R.M. Sanchez, G. Dunkelberger, N.I. Hernault, and T.A. Baginski. 1987. Chronic glaucoma selectively damages large optic nerve fibers. *Invest. Ophthalmol. Vis. Sci.* 28:913–920.

Quigley, H.A., G. Dunkelberger, and W.R. Green. 1988. Chronic human glaucoma causes selectively greater loss of large optic nerve fibers. *Ophthalmology.* 95:357–363.

Rice, D., and T. Curran. 2000. Disabled-1 is expressed in type AII amacrine clls in the mouse retina. *J. Comp. Neurol.* 424:327–338.

Robinson, G.A., and R.D. Madison. 2004. Axotomized mouse retinal ganglion cells containing melanopsin show enhanced survival, but not enhanced axon regrowth into a peripheral nerve graft. *Vision Res.* 44:2667–2674.

Rockhill, R., F. Daly, M. MacNeil, S. Brown, and R.H. Masland. 2002. The diversity of ganglion cells in a mammalian retina. *J. Neurosci.* 22:3831–3843. (published erratum appears in *J. Neurosci.* 2004. 24:2344)

Strettoi, E., E. Raviola, and R.F. Dacheux. 1992. Synaptic connections of the narrow-field, bistratified rod amacrine cell (AII) in the rabbit retina. *J. Comp. Neurol.* 325:152–168.

Strettoi, E., R.F. Dacheux, and E. Raviola. 1994. Cone bipolar cells as interneurons in the rod pathway of the rabbit retina. *J. Comp. Neurol.* 347:139–149.

Sun, W., N. Li, and S. He. 2002a. Large-scale morphological survey of mouse retinal ganglion cells. *J. Comp. Neurol.* 451:115–126.

Sun, W., N. Li, and S. He. 2002b. Large-scale morphological survey of rat retinal ganglion cells. *Vis. Neurosci.* 19:483–493.

Versaux-Botteri, C., J. Nguyen-Legros, A. Vigny, and N. Raoux. 1984. Morphology, density and distribution of tyrosine hydroxylase-like immunoreactive cells in the retina of mice. *Brain Res.* 301:192–197.

Whitmore, A.V., R.T. Libby, and S.W.M. John. 2005. Glaucoma: thinking in new ways—a role for autonomous axonal self-destruction and other compartmentalised processes? *Prog. Retin. Eye Res.* 24:639–662.